Proceedings of the ASME 2022 17th International Manufacturing Science and Engineering Conference
MSEC2022
June 27-July 1, 2022, West Lafayette, Indiana, USA

MSEC2022-85649

CHARACTERIZING THE CONDUCTIVITY OF AEROSOL JET PRINTED SILVER TRACES ON GLASS USING INTENSE PULSED LIGHT (IPL)

Connor Ferris
Department of Chemical Engineering, University of Kentucky
Lexington, KY

Dilan Ratnayake
Department of Electrical and Computer Engineering, University of Louisville
Louisville, KY

Alex Curry
Department of Electrical and Computer Engineering, University of Louisville
Louisville, KY

Danming Wei
Department of Electrical and Computer Engineering, University of Louisville
Louisville, KY

Erin Gerber
Department of Industrial Engineering, University of Louisville
Louisville, KY

Thad Druffel
JB Speed School of Engineering, University of Louisville
Louisville, KY

Kevin Walsh
Department of Electrical and Computer Engineering, University of Louisville
Louisville, KY

ABSTRACT

Aerosol Jet Printing is a novel micron-scale printing technology capable of handling a variety of materials due to a large print material viscosity range and high substrate standoff distance of 3-5 mm. To finalize the properties of printed materials, a form of post-processing is often required. A current widely applicable post-processing technique exists in traditional oven curing. However, oven curing greatly restricts the viable substrates as well as curing time. Intense Pulsed Light (IPL) offers the chance to greatly expand this substrate variety and decrease curing time. However, limited models currently exist to relate the finished material properties to the unique settings of current IPL technology. In this paper, an experiment is developed through a General Full Factorial Design of Experiments (DOE) model to characterize conductivity of Ag ink using IPL as a post processing technique. This is conducted through Novacentrix Ag ink (JSA426) by 3x3 mm Van der Pauw sensor pads cured using IPL. Sample pads were generated in triplicate over a range of Energy Levels, Counts and Durations for IPL and the resulting conductivity measured. The collected conductivity data was then analyzed using ANOVA to determine the significant interactions. From this, a regression model is developed to predict the conductivity for any Energy-Count-Duration value. The methods employed are applicable to any post-processing technique, and further optimization of the model is proposed for future work.

1. INTRODUCTION

The advance of micron-scale printing technologies can be exemplified by the emergence of Aerosol Jet Printing (AJP) in the late 1990's by the Defense Advanced Research Projects Agency (DARPA) [1]. AJP is a contactless, direct-write process for micron-scale printing on non-planar surfaces and a variety of substrates. This allows for generation of fine-pitch electronics [2] such as embedded sensors and resistors. This additive manufacturing process reflects the growing need for rapid prototyping at a miniaturized scale. These systems have primarily commercialized by companies such as Optomec Inc. in recent years [3], allowing for further research into the application of this technology to emerge.

The typical AJP process is divided into two primary components. The first component consists of an atomizer module, typically ultrasonic or pneumatic. Here, the substance is loaded and undergoes nebulization into droplets. The droplets form a dense mist that is then forced to flow by a carrier gas - also called the atomizer gas- into the second component, the deposition head. Here, a sheath gas, typically nitrogen, is used to condense the mist into the nozzle head, forming a tight stream. The stream is accelerated to a high velocity and forced onto the substrate. This process is shown below in Figure 1.

© 2022 by ASME

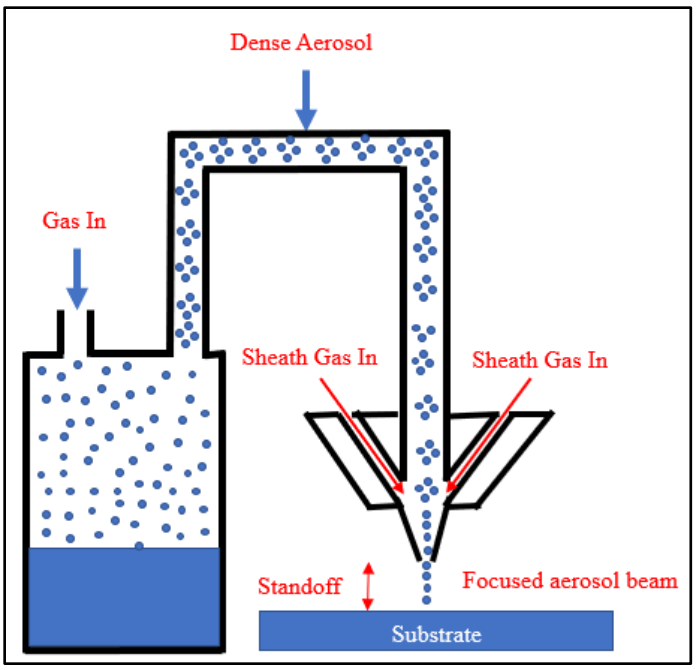

FIGURE 1: SCHEMATIC OF THE AEROSOL JET PRINTING PROCESS [4].

Typical AJP is capable of handling varied printing materials and substrates. The substrate variety is possible due to the to the high standoff distance of 3-5 mm [5], allowing for printing on non-planar surfaces. AJP systems allow for printing of both liquid and solid-state materials, typically converted to ink before loading. Typical printers are capable of a viscosity range of 0.7 to 2500 mPa·s [6] for liquids and solids with particle diameters less than 5 µm. Examples of such materials include polyimide, PEDOT, metals such as silver and platinum, and dielectrics such as epoxy and acrylic [6]–[9]. The printers can generate droplets of 1-5 µm diameter, allowing for features as small as 10 µm [7]. The feature size is typically modulated by nozzle selection.

Many printed features require a form of post-processing for stabilization. Several methods are typically utilized: traditional oven curing [10], Intense Pulsed Light (IPL) curing, or laser sintering [11]. Other methods, such as UV sintering, are also available [12]. The selection of post-processing technique limits both substrate variety and manufacturing time. Previously, our research group conducted experiments to characterize the use of oven thermal curing of Ag ink [4]. In this article, we investigate the use of IPL curing for high-conductivity silver ink on glass substrates, with the goal to develop a regression model between the curing parameters and silver conductivity. These parameters include Energy Level (J), Count and Duration (ms). If successful, the potential to integrate IPL into traditional AJP processes can greatly reduce curing time and increase substrate variety for printed electronic components. To better understand the relationship between the IPL curing parameters and the measured conductivity, a Design of Experiments (DOE) is utilized to determine the significant interactions.

2. MATERIALS AND METHODS

2.1 Aerosol Print Engine System

This experiment was conducted with the use of an Optomec Decathlon Print Engine. The engine is comprised of three components: the print module, process cabinet, and KEWA module software. This print module comprises an ultrasonic atomizer and deposition head. The ultrasonic atomizer generates pressure waves to create standing capillary waves with wavelength equal to the desired particle diameter. The crests break free of the waves to generate mist that is sent to the deposition head. The pressure waves are controlled by an ultrasonic transducer. The transducer current, atomizer flowrate, sheath flowrate, and system temperatures are controlled through the KEWA software. The KEWA software interfaces directly with the process control cabinet.

The printing motion is controlled by a six degree-of-freedom (6 DOF) slide deck stage, on which the substrate is mounted. The deck is moved below the print engine nozzle during printing. The printer was fitted with a 300 µm diameter nozzle for this experiment. The system is capable of printing down to one-tenth of the nozzle diameter, for this system 30 µm. The ink selected for this experiment was Novacentrix JSA-426 silver ink. This ink was selected for addition to a wider variety of substrates (ie. Kapton film) over other brands [13]. All print recipes were generated using this ink formula. The print module as well as the 6 DOF stage are shown below in Figure 2.

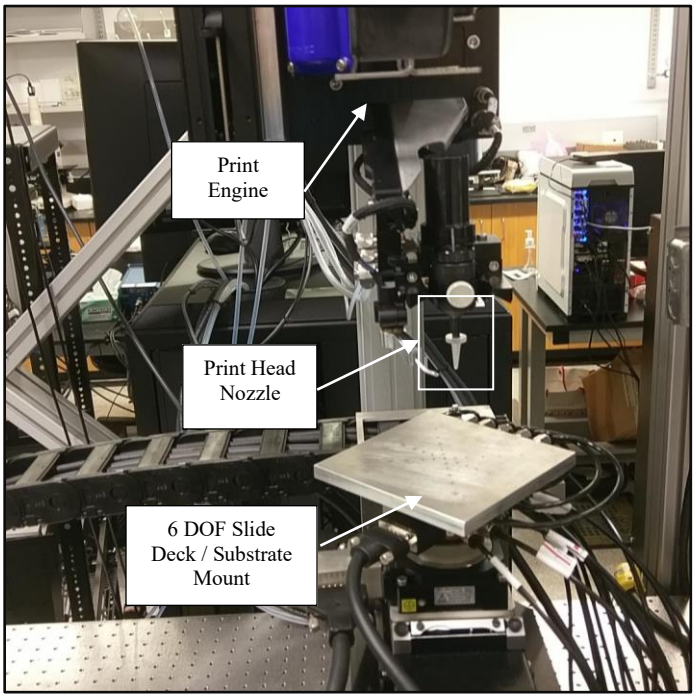

FIGURE 2: AEROSOL JET PRINTER WITH MOUNTED ULTRASONIC ATOMIZER MODULE. PADS WERE PRINTED UTILIZING A SIX-DEGREE-OF-FREEDOM (6 DOF) SLIDE DECK UNDERNEATH A STATIONARY PRINT HEAD NOZZLE. PRINT HEAD NOZZLE IS HIGHLIGHED ABOVE THE SLIDE DECK.

© 2022 by ASME

2.2 Print Recipes and Procedures

The printing parameters were set within the KEWA module software. The atomizer flowrate was set to a value of 20 sccm. The sheath flowrate was set to a value of 130 sccm. The transducer current was set to 500 mA and the Ultrasonic bath temperature to 23ºC, close to the ambient temperature. The UA heater was set to a value of 27ºC. The viscosity of the Novacentrix ink required a dilution rate of 2:1 of Ink:DI water in order to reach the ultrasonic atomizer range of 1-10 cP. This recipe produced lines of 50 μm average width when viewed under a microscope. The environmental conditions of the printing remained between 69ºF and 71ºF. These conditions were susceptible to generating variation in the line morphology, requiring adjustment to the process recipe. This primarily impacted the line width and continuity. Line widths of 45 to 55 μm widths were deemed acceptable for printing. Prior to attempting printing, line widths were checked and verified to ensure that the width specifications were met. An example of the test printed lines is shown in Figure 3.

The stage speed was set to 10 mm/s and stage acceleration to 50 mm/s^2. These were adjusted to limit vibration in the slide deck during motion to prevent uneven or oscillatory line structures. Printing designs were generated using CAD software and uploaded to the slide deck. The printing was conducted using an overlapping serpentine structure, wherein each line is printed individually then the position of the printer reset for the next line in the code. This was accomplished using a shutter that blocked the mist stream exiting the nozzle while the deck moved to the start of each individual line.

The shape was chosen as a 3x3 mm Van der Pauw sensor pad. To ensure a continuous pad, the periodicity of the printed lines was modulated to determine the maximum value to minimize print time and total pad thickness. Iterations on the sensor pad design were conducted using a variety of serpentine structures to further assess the optimal pad design for thickness profile. The tested designs included an overlapping parallel line printed pad, a crosshatched design, and an overlapping parallel line pad printed along the pad's diagonal. Of these designs, the diagonal structure was selected for its ease of printing and consistent thickness profile. The periodicity was selected to be 40 μm. The optimal design was a serpentine pad with lines printed at 45º with outlined pad edges. Pads were printed on 1 mm thick microscope glass slides. After printing, pads were then loaded into the IPL for post-process sintering. Both a magnified example of a typical individual line structure as well as fully printed pad are shown in Figure 3.

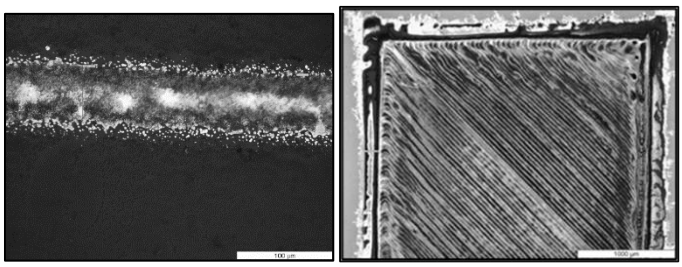

FIGURE 3: PRINTED SILVER LINE TEST UNDER 5X MAGNIFICATION (LEFT). PRINTED TEST SENSOR PAD AT 5X MAGNIFICATION (RIGHT). SENSOR PADS WERE CREATED USING OVERLAPPING LINE STRUCTURES TO CREATE A CONTINOUS SURFACE, RESULTING IN AN EVEN THICKNESS PROFILE.

2.3 Sintering Process

All samples were printed in a single batch. Pads were then loaded in print order into the IPL system for curing to ensure all samples had equal drying time. IPL curing utilizes xenon flash lamps to emit a wide wavelength of light over the substrate by discharging a capacitor [14], allowing for curing of wide areas of the substrate compared to laser sintering. Both processes cause the removal of solvent from the silver nanoparticles found in commercial inks. The silver nanoparticles then absorb energy and decrease the particle distance, resulting in lattice diffusion and lowered interstitial boundary distance to generate a continuous structure [15]. If the absorbed energy does not fully remove the solvent, the electrical resistance of the pads increases and lowers the resulting conductivity [16]. If too much energy is absorbed, the polymer binding the ink to the substrate is destroyed, resulting in delamination of the pad. These phenomena represent the boundary conditions for the IPL curing.

The IPL system has four parameters to set before curing: Energy (J), Count, Duration (ms), and Delay (s). The Energy level modulates the magnitude sent to the sampleYe. The Count denotes the number of emitted pulses of light. The Duration sets the emission time, and the Delay sets the time between each emission. The energy absorbed by the substrate is controlled through the Energy, Count and Duration of emissions. The Delay does not impact the absorbed energy on the nanoparticles, and was selected as a controlled variable to remain constant at 1 s.

Preliminary tests revealed high resistance in pads cured at an Energy level of 200 J. Pads cured at an Energy level of 800 J exhibited destruction of the ink surface due to delamination. Further tests modulation Count and Duration at an Energy level of 500 J revealed delamination occurs at Durations exceeding 1000 ms and Counts exceeding 9. This experiment employed a Design of Experiments (DOE) method to optimize the conductivity of silver traces printed on glass substrates. The preliminary tests were used in the generation of the parameter ranges examined.

2.4 Conductivity Measurement

The conductivity calculations of this experiment employ the Van der Pauw method. This method was developed in 1958 for thin-film samples, in which the sample thickness is significantly

© 2022 by ASME

smaller than the length and width. Four probes are placed uniformly along the boundary of the sample. Current is induced in two adjacent probes, and the corresponding change in voltage is measured across the two remaining probes, shown in Figure 4. These values are employed with the use of Equation 1 to determine the film resistivity.

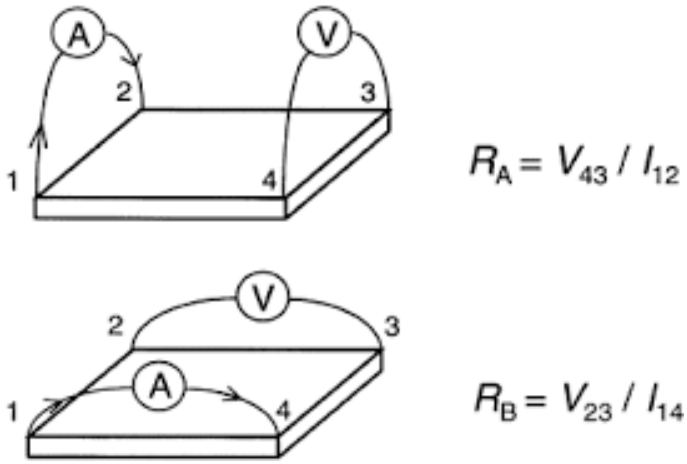

FIGURE 4: DIAGRAM FOR VAN DER PAUW MEASUREMENT OF THIN-FILM APPLICATIONS [4]. SENSOR PAD TESTS WERE CONDUCTED UTILIZING THE LAYOUT SHOWN ABOVE WITH IDENTICAL POINT NUMBERING.

$$\rho = \frac{\pi}{\ln(2)} \boldsymbol{t} \frac{V_{34}}{I_{12}} = 4.53 \boldsymbol{t} \frac{V_{34}}{I_{12}} \quad (1)$$

Where t is the thickness of the film, I the induced current, and V the measured voltage. The conductivity is then calculated using Equation 2 as:

$$\sigma = \frac{1}{\boldsymbol{\rho}} \quad (2)$$

The conductivity was measured by the use of a four-point probe station with micromanipulator probes fitted with 0.35 µm diameter tungsten probes. A current of 4.53 mA was induced across one edge of the sample with a Keithley 224 Programmable Current Source. The resulting voltage change on the opposite end was measured with an Aligent 6¬1/2 Digit Multimeter. The experiment setup is depicted in Figure 5.

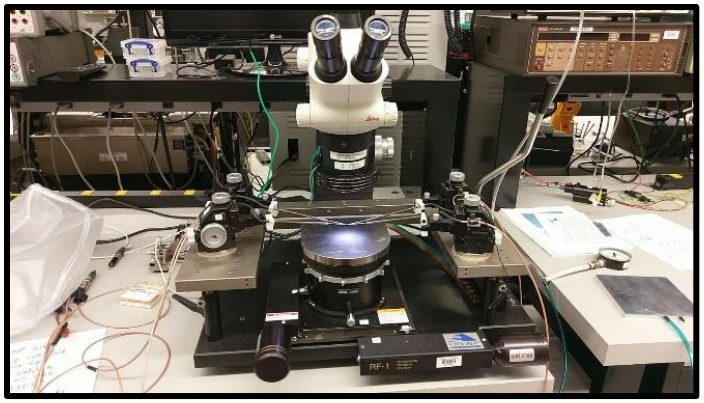

FIGURE 5: FOUR-POINT PROBE STATION FITTED WITH 0.35 DIAMETER MM TUNGSTEN PROBES.

3. RESULTS AND DISCUSSION

As discussed in the previous section, 3x3 mm Novacentrix silver ink sensor pads were printed onto microscope glass slides and cured under IPL. Each sample consisted of three sensor pads to generate replicate trials. Energy values were measured at 300, 500 and 700 J. Durations were measured at 250, 500 and 750 ms. Counts were measured at 3, 6 and 9. A total of 27 samples were printed in triplicate for a total of 81 sensor pads. The average thickness of each pad was measured across its vertical orientation using a DekTak Profilometer shown in Figure 6. Variation in thickness is caused due to the overlapping serpentine structure used to generate the design. The large peak of thickness observed at the start of each pad is attributed to the shutter disengaging at the start of each printed line. Overspray is generated at the beginning of each line due to the continuous stream of mist generated by the printer blocked by the shutter before each pass. Thickness was averaged across the entire pad length. Edge thickness variations were included in this summation, potentially resulting in a lower measured conductivity.

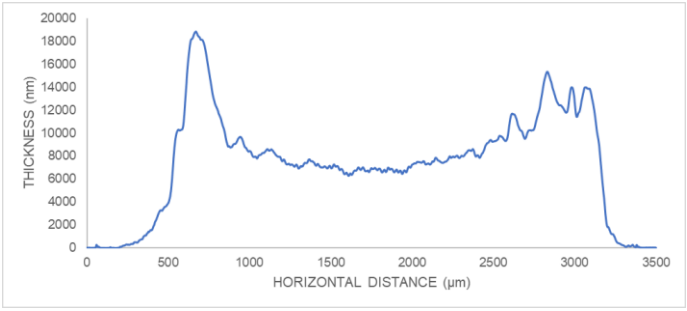

FIGURE 6: DEKTAK PROFILE READOUT ACROSS THE VERTICAL ORIENTATION OF A 3X3 MILIMETER PAD. THE HATCH SPACING WAS SET TO 40 µm FOR THIS DESIGN.

The four-point probe station was then used in conjunction with the Van der Pauw method to generate conductivity data for each pad. Probes were placed on the edge of each pad in accordance with the Van der Pauw method and individual voltage readings were taken. Probes were tested both along the

© 2022 by ASME

edge profile and within the middle of the pad and produced no significant difference in readings. Samples labeled as 'NO RESPONSE' represent pads where insufficient curing was encountered, resulting in high resistance and conductivity was unable to be measured. For the purposes of statistical analysis, these pads are represented as a zero value for conductivity. Previous results have indicated the conductivity of cured silver at 200 ºC overnight is 7.05E+06 $\frac{1}{\Omega M}$ and is used as the standard for this experiment [4]. The results of the DOE are shown in Figure 7 and an ANOVA General Linear Model statistical analysis on this data is shown in Figure 8.

Energy (J)	Count	Duration (ms)	Conductivity Response (Ω^{-1} m^{-1})
300	3	250	NO RESPONSE
		500	4.523E+04
		750	1.418E+05
	6	250	NO RESPONSE
		500	3.109E+04
		750	1.834E+05
	9	250	NO RESPONSE
		500	NO RESPONSE
		750	*2.156E+05*
500	3	250	NO RESPONSE
		500	1.622E+05
		750	3.335E+05
	6	250	1.451E+05
		500	2.552E+05
		750	4.569E+05
	9	250	1.496E+05
		500	2.435E+05
		750	*4.741E+05*
700	3	250	3.028E+05
		500	2.943E+05
		750	4.956E+05
	6	250	2.471E+05
		500	5.691E+05
		750	7.412E+05
	9	250	3.901E+05
		500	5.138E+05
		750	*8.019E+05*
Cured in oven overnight at 200 C			**7.05E+06**
Bulk Silver			**6.30E+07**

FIGURE 7: EXPERIMENTAL DATA FROM THE 27 RANDOMIZED SAMPLES. DATA POINTS WERE AVERAGED FROM INDEPENDENT REPLICATE TRIALS. COMPARISON VALUES FOR TYPICAL OVEN CURED SILVER AND BULK SILVER WERE SOURCED FROM PREVIOUS EXPERIMENTS. VALUES IN ITALICS REPRESENT THE HIGHEST RECORDED CONDUCTIVITY VALUE FOR EACH ENERGY LEVEL.

Source	DF	F-Value	P-Value
Energy (J)	2	1099.29	0.000
Count	2	92.74	0.000
Duration (ms)	2	550.67	0.000
Energy (J)*Count	4	22.7	0.000
Energy (J)*Duration (ms)	4	20.64	0.000
Count*Duration (ms)	4	11.26	0.000
Energy (J)*Count*Duration (ms)	8	9.2	0.000

FIGURE 8: TABULATED VALUES FROM MINITAB OUTPUT OF THE MODEL SUMMARY BY ANOVA ANALYSIS. ANALYSIS OF VARIANCE IS UTILIZED TO DETERMINE IF INTERACTIONS BETWEEN THE INDICATED VARIABLES ARE STATISTICALLY SIGNIFICANT IN THE OVERAL REGRESSION MODEL. THE THRESHOLD FOR SIGNIFICANT RESULTS IS SET AT A P-VALUE OF 0.05 (5%).

In general, all samples that did not suffer delamination were unable to reach the conductivity of the same silver ink cured in an oven overnight. Values cured at the threshold values showed values approaching the order of magnitude of 10^6 $\Omega^{-1}m^{-1}$, with the largest recorded conductivity being 8.338E+05 $\Omega^{-1}m^{-1}$ at an Energy level of 700 J, Count of 9 and Duration of 750 ms.

The threshold for significance is taken as a p-value of 0.05 (5%). The ANOVA reveals that Duration, Count and Delay all significantly affect the conductivity of cured samples, exhibiting p-values less than 0.0001 (0.1%). Furthermore, the interactions between each of these parameters exhibit similar p-values, indicating that there is a complex relationship to the factors and their levels.

Next, a Tukey Pairwise Comparison was run on the three-way interaction. This analysis shows that there are two combinations of the three factors tested that will provide the statistically signification maximization for the conductivity. Both maximizing combinations utilize the highest Energy level of 700 J and Duration of 750 ms. Counts of either 6 or 9 may be used to with these settings to obtain maximized conductivity measures. This suggests the model may not capture the highest possible IPL curing parameters before delamination is encountered, and therefore the maximum conductivity may not be part of the data set. The analysis, however, verifies that the conductivity is minimized at the lowest testing parameters, implying the conductivity is positively correlated with Energy, Duration and Count of the IPL.

Based on the complexity of significant interactions found in the ANOVA, a best subsets regression analysis was run, and a variety of well-fitting regressions models were attempted. The final selected regression model for the system is shown in Equation 3.

$$\sigma = (-1.30e5) + (2.07e4)(\boldsymbol{C}) + (78.89)(\boldsymbol{E} * \boldsymbol{C}) + (1.13)(\boldsymbol{E} * \boldsymbol{D}) \quad (3)$$

Where C is the count, E is the Energy (J), and D is the Duration (ms). The Residual plots for this regression model are shown in Figure 9. Based on these plots, all parametric assumptions can be accepted for the model.

© 2022 by ASME

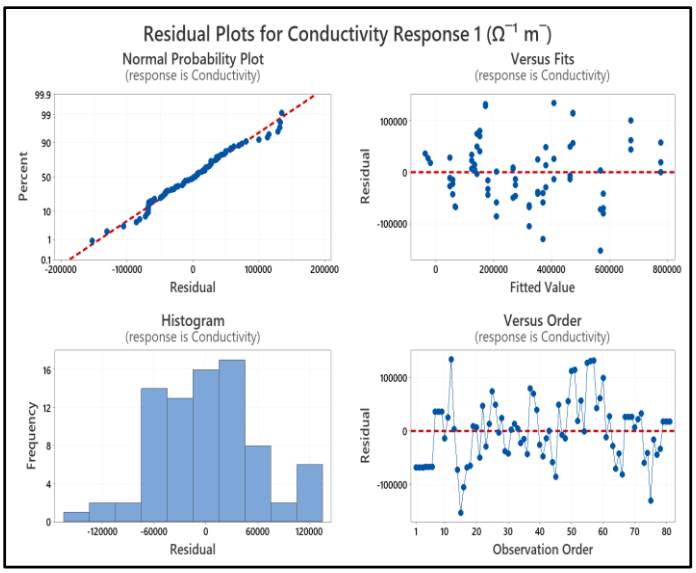

FIGURE 9: RESIDUAL ANALYSIS FOR REGRESSION MODEL ADEQUACY. CONDUCTIVITY IS TAKEN AS THE RESPONSE.

The adjusted coefficient of determination for this model was 0.9255, suggesting a sufficient fit for the conductivity data collected. By comparison, the general linear regression analysis of the IPL settings without interaction found an adjusted coefficient of determination of 0.8851, indicating that analysis of the parameters separately is insufficient. In the model, the interaction of Energy and Count (E*C) is representative of the magnitude of the absorbed energy. The interaction of Energy and Duration (E*D) is representative of the total exposure time of energy onto the silver ink. Both parameters have significant influence on the energy absorbed by the nanoparticles during the curing process. While this model does not capture the interaction of Count and Duration (C*D), this interaction was the second-least significant interaction according to the ANOVA output. Furthermore, the total interaction of Energy, Count and Duration (E*C*D) had the least overall significance to the conductivity.

To analyze model adequacy, the residuals between the model and DOE trials were analyzed. The lack of correlations between the residuals indicates time-based factors did not impact the data set. When utilizing parametric analysis such as these, residuals should take the form of a normal distribution with a mean of zero and constant variance. As shown in Figure 12, the residuals lack a fully defined normal distribution with a mean below zero. This implies there may be further potential optimization of the model.

The work revealed one deviation of the expected result in the magnitude of the measured conductivity results. As mentioned prior, previous data found silver cured overnight at 200ºC has a conductivity of 7.05e6 $\Omega^{-1}m^{-1}$. Furthermore, the conductivity of bulk silver is known to be 6.30e7 $\Omega^{-1}m^{-1}$. While the measured trials exhibit the positive correlation between increasing IPL settings and conductivity, they exhibit conductivity on the order of 10^6 $\Omega^{-1}m^{-1}$. Combined with the results of the Tukey Test, this suggests a need for further optimization of the IPL parameters to approach the threshold of oven cured samples.

An explanation for this lower value of conductivity is the thickness of the pads. The observed thickness of the pads was 3000-5000 nm. Previous experiments have yielded an expected thickness of 1000-2000 nm. As the data exhibit the same trends as previous curing experiments [4], this indicates that the sample may have only exhibited partial curing on the top layer. This would imply that the portion of the top layer of pad would be comparable to the expected thickness and increase the calculated conductivity. Another explanation, however, is that the variation in the pad thickness was caused by the continuous printing, resulting in changes to line morphology. To test this assumption, an analysis was run of the pad thickness versus the run order of the samples, shown in Figure 10.

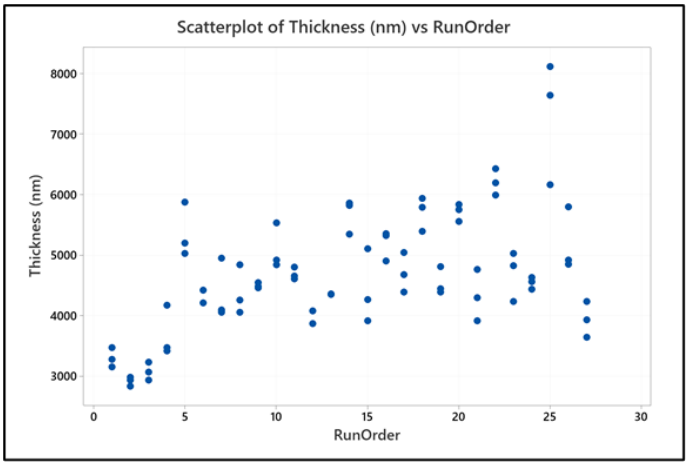

FIGURE 10: SCATTERPLOT ANALYSIS OF PAD THICKNESS (NM) VERSUS DOE RUN ORDER. THIS ANALYSIS IS UTILIZED TO SHOW THE INDIVIDUAL RUN ORDER OF THE TESTS DID NOT EFFECT THE OVERALL THICKNESS OF THE PADS.

Analysis reveals no strong correlation was present between the Run Order of the samples during the DOE and the thickness of the pads. It is known that the morphology of the lines change as the printer is used continuously, yet this analysis indicates it is not a significant factor. Therefore, to verify if the entire pad was cured at the time of analysis, SEM imaging is recommended for future work.

4. CONCLUSIONS

In summary, the conductivity of AJP silver traces under IPL curing was analyzed using a General Full Factorial DOE Model with three factors at three levels each. Trials was executed using Novacentrix silver ink with an Optomec Decathlon Print Engine by 3x3 mm Van der Pauw sensor pads on microscope glass slide substrate. The Van der Pauw method was employed to determine the conductivity of the pads and analyzed first through as ANOVA General Linear Model. Further analysis (via a post-hoc Tukey test) reveals the model is maximized at the highest tested parameters, indicating the maximum conductivity may lie outside the data set. A regression model was selected and found

© 2022 by ASME

appropriate for predicting conductivity within Energy ranges of 300 to 700 J, Durations of 250 to 750 ms, and Counts of 3 to 9. Furthermore, the order of magnitude discrepancy between previous oven cured experiments suggests the pad thickness may have other unanalyzed impacts on the sample. The methods shown here are not specific to the tested ink or post-processing method and may be used to further characterize other methods such as laser sintering.

From these results arise areas for potential future work. The impact of Delay was not measured on the system, as a constant delay was utilized within the DOE. Future characterization should determine if this parameter is significant at predicting the conductivity of the sample by including it as a factor in experimental trials. Furthermore, more robust thickness analysis should be considered for other post-processing experiments, such as SEM imaging.

ACKNOWLEDGEMENTS

This research was supposed by National Science Foundation Award EECS-1950137 for the IMPACT-NG REU program, which is a part of the NSF National Nanotechnology Coordination Infrastructure (NNCI) and National Science Foundation Award EECS-2025075. Additional support was given by Kentucky Multiscale and the staff of the Kentucky Micro/Nano Technology Center (MNTC).

© 2022 by ASME

REFERENCES

[1]M. Maher, A. Smith, and J. Margiotta, “A synopsis of the Defense Advanced Research Projects Agency (DARPA) investment in additive manufacture and what challenges remain,” San Francisco, California, United States, Mar. 2014, p. 897002. doi: 10.1117/12.2044725.

[2]C. Goth, S. Putzo, and J. Franke, “Aerosol Jet printing on rapid prototyping materials for fine pitch electronic applications,” in *2011 IEEE 61st Electronic Components and Technology Conference (ECTC)*, May 2011, pp. 1211–1216. doi: 10.1109/ECTC.2011.5898664.

[3]N. Wilkinson, M. Smith, R. Kay, and R. Harris, “A review of aerosol jet printing—a non-traditional hybrid process for micro-manufacturing,” *IJAMT*, vol. 105, pp. 4599–4619, Dec. 2019, doi: 10.1007/s00170-019-03438-2.

[4]D. Ratnayake, A. T. Curry, C. Qu, J. Usher, and K. Walsh, “CHARACTERIZING THE CONDUCTIVITY OF AEROSOL JET PRINTED SILVER FEATURES ON GLASS,” in *Smart Materials and Structures*, Virtual, Jun. 2021, pp. 1–6.

[5]“AEROSOL JET PRINTED ELECTRONICS OVERVIEW,” *OPTOMEC*.

[6]W. Verheecke, M. Dyck, F. Vogeler, A. Voet, and H. Valkenaers, “Optimizing aerosol jet® printing of sil-ver interconnections on polyimide film for embedded electronics applications,” Tallinn, Estonia, 2012, pp. 373–379. Accessed: Jul. 27, 2021. [Online]. Available: https://www.semanticscholar.org/paper/Optimizing-aerosol-jet%C2%AE-printing-of-sil-ver-on-film-Verheecke-Dyck/bb1b260fb34403e74a34041a930e67e5d14dc198

[7]A. A. Gupta, A. Bolduc, S. G. Cloutier, and R. Izquierdo, “Aerosol Jet Printing for printed electronics rapid prototyping,” in *2016 IEEE International Symposium on Circuits and Systems (ISCAS)*, May 2016, pp. 866–869. doi: 10.1109/ISCAS.2016.7527378.

[8]B. Wang, H. Zhang, J. P. Choi, S. K. Moon, B. Lee, and J. Koo, “A Post-Treatment Method to Enhance the Property of Aerosol Jet Printed Electric Circuit on 3D Printed Substrate,” *Materials*, vol. 13, no. 24, Art. no. 24, Jan. 2020, doi: 10.3390/ma13245602.

[9]M. Hedges and A. B. Marin, “3D Aerosol Jet® Printing - Adding Electronics Functionality to RP/RM,” Berlin, Mar. 2012, pp. 1–5.

[10]M. Serpelloni, E. Cantù, M. Borghetti, and E. Sardini, “Printed Smart Devices on Cellulose-Based Materials by means of Aerosol-Jet Printing and Photonic Curing,” *Sensors*, vol. 20, no. 3, Art. no. 3, Jan. 2020, doi: 10.3390/s20030841.

[11]C. E. Hajjaji, N. Delhote, S. Verdeyme, M. Piechowiak, L. Boyer, and O. Durand, “Optimization of the conductivity of microwave components printed by inkjet and aerosol jet on polymeric substrates by IPL and laser sintering,” *International Journal of Microwave and Wireless Technologies*, pp. 1–11, Apr. 2021, doi: 10.1017/S175907872100043X.

[12]C. Crump, V. Gjokaj, B. Wright, J. Papapolymerou, J. D. Albrecht, and P. Chahal, “UV Flash Sintering of Aerosol Jet Printed Silver Conductors for Microwave Circuit Applications,” *IEEE Transactions on Components, Packaging and Manufacturing Technology*, vol. 11, no. 2, pp. 342–350, Feb. 2021, doi: 10.1109/TCPMT.2020.3047055.

[13]“Metalon JS-A426 datasheet,” *www.NovaCentrix.com*.

[14]J. Niittynen, E. Sowade, H. Kang, R. R. Baumann, and M. Mäntysalo, “Comparison of laser and intense pulsed light sintering (IPL) for inkjet-printed copper nanoparticle layers,” *Sci Rep*, vol. 5, no. 1, p. 8832, Mar. 2015, doi: 10.1038/srep08832.

[15]Y. Zhang, L. Wu, X. Guo, Y.-G. Jung, and J. Zhang, “Molecular dynamics simulation of electrical resistivity in sintering process of nanoparticle silver inks,” *Computational Materials Science*, vol. 125, pp. 105–109, Dec. 2016, doi: 10.1016/j.commatsci.2016.08.047.

[16]L. Makkonen, “On the Methods To Determine Surface Energies,” *Langmuir*, vol. 16, no. 20, pp. 7669–7672, Oct. 2000, doi: 10.1021/la990815p.

© 2022 by ASME